Phonon Instabilities and the Ideal Strength of Aluminum

D. M. Clatterbuck,[1,2] C. R. Krenn,[4] Marvin L. Cohen,[1,3] and J. W. Morris, Jr.[1,3,*]

[1]*Materials Sciences Division, Lawrence Berkeley National Lab, Berkeley, California 94720, USA*
[2]*Department of Materials Science and Engineering, UC Berkeley, Berkeley, California 94720, USA*
[3]*Department of Physics, UC Berkeley, Berkeley, California 94720, USA*
[4]*Chemistry and Material Science Division, Lawrence Livermore National Laboratory, Livermore, California 94551, USA*

(Received 31 March 2003; published 23 September 2003)

We have calculated the phonon spectra of aluminum as a function of strain using density functional perturbation theory for ⟨110⟩, ⟨100⟩, and ⟨111⟩ uniaxial tension, as well as relaxed ⟨112⟩{111} shear. In all four cases, phonon instabilities occur at points away from the center of the Brillouin zone and intrude before the material becomes unstable according to elastic stability criteria. This is the first time the ideal strength of a metal has been shown to be dictated by instabilities in the acoustic phonon spectra. We go on to describe the crystallography of the unstable modes, all of which are shear in character. This work further suggests that shear failure is an inherent property of aluminum even in an initially dislocation-free perfect crystal.

DOI: 10.1103/PhysRevLett.91.135501 PACS numbers: 63.20.Dj, 62.20.–x, 64.70.Kb, 71.15.Mb

The ideal strength of a material is the stress at which a perfect crystal becomes mechanically unstable [1,2] and sets an upper bound on the strength the material can attain in practice. The ideal strength is also relevant experimentally in situations which probe small, defect-free regions of a material as in nanoindentation. In fact, it has been demonstrated that the strengths obtained in nanoindentation can be quantitatively computed with the use of first principles electronic structure calculations coupled with finite element simulations [3].

Almost all previous studies of the ideal strength have focused on mechanical instabilities whose eigenmodes correspond to homogeneous deformation; however, eigenmodes corresponding to inhomogeneous deformation are also possible [4]. For example, it is possible for a material to become unstable with respect to vibrational modes before it becomes elastically unstable [5]. In fact this has been shown to be important for understanding the anomalous hardness of TiC in relation to TiN [6,7]. In this case, the strength of TiN is limited by the instability of an optical phonon. This early instability decreases its strength relative to that of TiC, which does not exhibit this type of instability. Other prior work in this area includes that of Li and Yip who used an empirical bond order potential to locate phonon instabilities in SiC under pure shear [8]. This paper provides the first example of a simple metal in which the ideal strength is limited by phonon instabilities.

Stability requires that the energies of phonons be positive for all wave vectors in the Brillouin zone [8,9]. A phonon that lowers the energy of the crystal will grow in amplitude until the structure is driven to a new stable state. The incremental atomic displacements of the unstable phonon mode can be determined from the eigenvectors of the dynamical matrix. The unstable eigenvector indicates the crystallographic nature of the initial instability, which may, of course, become very different in nature as it develops finite amplitude.

In our calculations, total energies and Hellmann-Feynman stresses were calculated using density functional theory while phonon frequencies were computed with density functional perturbation theory [10] all within the local density approximation (LDA) [11–13]. The plane-wave pseudopotential method as implemented within the ABINIT code [14] was used along with the Goedecker-Teter-Hutter Al pseudopotential [13] which required a plane-wave cutoff of 32 Ry. The "cold smearing" method of Marzari [15] was used for Brillouin zone (BZ) integrations with a smearing parameter of 0.04 Ry. The total energy and stress calculations used a $16 \times 16 \times 16$ Monkhorst-Pack (MP) [16] k-point grid. The error in the stresses due to the basis set size, smearing parameter, and k-point grid was found to be ~ 0.1 GPa based on convergence studies.

The quasistatic ideal strength and relaxed loading path in the various directions was determined using a method described in detail previously [17,18]. The lattice vectors were incrementally deformed in the direction of the applied stress. At each step the structure was relaxed such that all of the components of the Hellmann-Feynman stress tensor orthogonal to the applied stress were less than 0.1 GPa. In order to avoid a dependence of the quasistatic ideal strength on the loading mechanism [19], we define the strength according to the limits of internal stability derived by Morris and Krenn [20].

Our phonon studies employed the following method. First, for several structures along each relaxed loading path, an initial search for unstable modes was performed by computing the dynamical matrix on a $6 \times 6 \times 6$ MP grid of points in the irreducible BZ using a $12 \times 12 \times 12$ MP grid of k points. From this information, the interatomic force constants were extracted and used to

TABLE I. Calculated and experimental lattice parameter and elastic constants of fcc Al. Experimental lattice parameter was extrapolated to 4 K using low temperature thermal expansion data [22]. Experimental elastic constants at 4 K are from Ref. [23].

	Calculated	Experimental (4 K)	% Error
a_0 (Å)	3.98	4.02	−1.1
c_{11} (GPa)	117.5	114.3	2.8
c_{12} (GPa)	63.5	61.9	2.6
c_{44} (GPa)	35.5	31.6	12.3
B (GPa)	81.5	79.4	2.7

interpolate the phonon frequencies [21] in order to find unstable modes and determine their locations in the BZ. The phonon frequencies as a function of strain were then directly recalculated (without interpolation) along the high symmetry directions in the BZ which exhibited unstable modes using a $20 \times 20 \times 20$ MP grid of k points in order to obtain high accuracy frequencies (converged to ~0.1 THz). These higher accuracy frequencies were within 1 THz of those calculated earlier, indicating that the initial search parameters were reasonable.

Table I gives the results of benchmark calculations which were used to check the quality of the pseudopotential. The lattice parameter was found to be 1% too small while the elastic constants were 2%–12% too big compared to experiment, typical of LDA calculations which tend to overbind. The phonon spectra of the equilibrium fcc structure computed using the 0 K LDA lattice parameter is in excellent agreement with the experimental data obtained at 80 K as shown in Fig. 1.

Figure 2 presents the stress-strain curves for Al in ⟨110⟩, ⟨111⟩, and ⟨100⟩ tension as well as ⟨112⟩{111} shear (we shall discuss the details of the quasistatic loading behavior of Al elsewhere). The open circles indicate the locations of the phonon instabilities described below. In each case the phonon instability occurs before the peak of the stress-strain curve; however, in ⟨110⟩ tension and ⟨112⟩{111} shear the phonon instabilities are located at strains much closer to the peak than is the case in ⟨100⟩ and ⟨111⟩ tension. This indicates that the phonon instabilities in ⟨100⟩ and ⟨111⟩ tension significantly reduce the

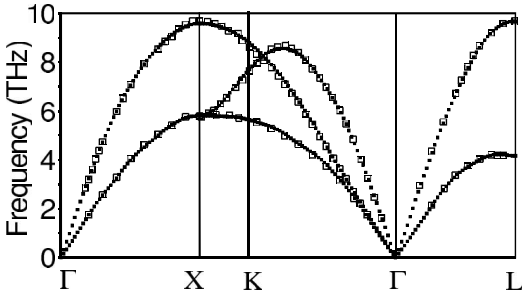

FIG. 1. Phonon dispersion of Al measured experimentally at 80 K (open symbols) [24] and calculated using the 0 K LDA lattice parameter (filled symbols).

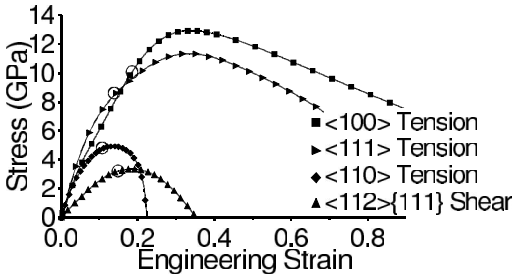

FIG. 2. Stress-strain curves for ⟨110⟩, ⟨100⟩, and ⟨111⟩ uniaxial tension as well as relaxed ⟨112⟩{111} shear. Open circles indicate the location of phonon instabilities. The lines are guides for the eye. In all loading configurations phonon instabilities occur before the material becomes elastically unstable.

ideal strength in these directions, while the value of the ideal strength in ⟨110⟩ tension and ⟨112⟩{111} shear is not strongly affected by the phonon instabilities as summarized in Table II. We note that our calculation of the quasistatic ideal shear strength (3.3 GPa) is in good agreement with the recent work of Yip and co-workers [25] who obtained 2.84 GPa using the generalized gradient approximation (GGA) and reported that the LDA produced strengths 10%–20% higher. (As noted in Ref. [25], this value is significantly larger than the first calculation of the ideal shear strength of Al [18,26].) Although the stresses resulting from the LDA and GGA differ, we find that the strains corresponding to the ideal strength and the associated stress-free saddle point structures are not as sensitive to the gradient corrections. Since the phonon instabilities described below appear to be determined by critical strains [27], we expect that the GGA would produce results similar to our LDA calculations in terms of the instability strain while producing lower stresses at the corresponding strains. As such, the LDA results serve as a more conservative upper bound on the strength.

The phonon spectra are shown as a function of strain in Figs. 3–5. We have included only the high symmetry

TABLE II. Stresses and strains associated with phonon instabilities as compared to the peak in the stress-strain curves shown in Fig. 2. Also shown are the shear plane and displacement associated with the phonon instabilities.

Loading configuration	Phonon instability σ (GPa)	e	Peak stress-strain curve σ (GPa)	e	Shear system of instability
[110] tension	4.89	0.115	4.92	0.140	$[\bar{1}12](111)$
$[11\bar{2}](111)$ shear	3.16	0.145	3.33	0.185	$[\bar{1}12](111)$
[001] tension	9.20	0.170	12.92	0.340	[001](100)
					$[1\bar{1}0](11\bar{1})$
[111] tension	8.95	0.150	11.30	0.330	[111](001)
					[111](110)
					$[111](\bar{1}10)$
					$[111](\bar{1}11)$

directions in the Brillouin zone along which phonon instabilities were found to occur. Also, only the branch corresponding to the polarization which goes unstable is shown to simplify the figures. For convenience we use the negative y axis to plot imaginary frequencies. In general we see the softening of various phonon branches occurring gradually as the strain is increased. At the largest strains, the initial slope of the dispersion curves is negative. When this happens the material is unstable with respect to homogeneous deformation (long wavelength distortions) and is thus elastically unstable.

In Fig. 3(a) we see that in [110] tension a phonon instability develops around 11% strain. At this strain, the instability has a $[111]/3$ wave vector, but larger wave vectors quickly become unstable as the strain is increased slightly. Analysis of the eigenvectors of the dynamical matrix indicates that the unstable mode corresponds to displacements in approximately the $[\bar{1}12]$ direction. Thus the failure is a $[\bar{1}12](111)$ shear failure in which the displacements have a periodicity of 3 (111) planes. Interestingly, this periodicity is commiserate with the *ABCABC* stacking of the (111) planes found in the fcc structure.

In the case of an applied $[11\bar{2}](111)$ shear, the instability first occurs at a wave vector between $[111]/3$ and $[111]/2$ at an engineering shear strain of 14% [Fig. 3(b)]. The unstable mode has displacements in the $[\bar{1}12]$ direction resulting in a $[\bar{1}12](111)$ shear failure with a periodicity of 2 or 3 (111) planes. Independent frozen phonon calculations confirmed the existence and location of the instability at 14% applied shear strain.

The geometry of the instability that occurs in $\langle 110\rangle$ tension is identical to that found in $\langle 112\rangle\{111\}$ shear [Fig. 3(c)]. This is probably because $\langle 110\rangle$ tension can be visualized as a superposition of $\langle 112\rangle\{111\}$ shear and an expansion perpendicular to the shear plane. The two deformation modes also produce very similar elastic instabilities. On further deformation both loading configurations eventually produce the same stress-free body-centered-tetragonal structure (which is a saddle point on the energy-strain hypersurface).

A different type of instability is found in [001] tension. In this case instabilities occur with wave vectors in two separate regions of the Brillouin zone. At around 17% strain an instability occurs at $[11\bar{1}]/2$ followed by another at around 18% near $2[100]/3$. We find that the displacements in the two cases correspond to periodic $[1\bar{1}0](11\bar{2})$ shear and [001](100) shear, respectively. A schematic of the crystallography of these instabilities is shown in Fig. 4(b). Increased strain causes the region of unstable wave vectors to grow significantly until the material becomes elastically unstable at strains that correspond to the peak of the stress-strain curve.

Of the four loading configurations studied, the electronic origin of this instability is the most clear. At the strain corresponding to the phonon instability the bottom of the second band at the X point ([100] direction) has increased to the extent that it has reached the Fermi level and thus has been depopulated [Fig. 4(c)]. This can also be

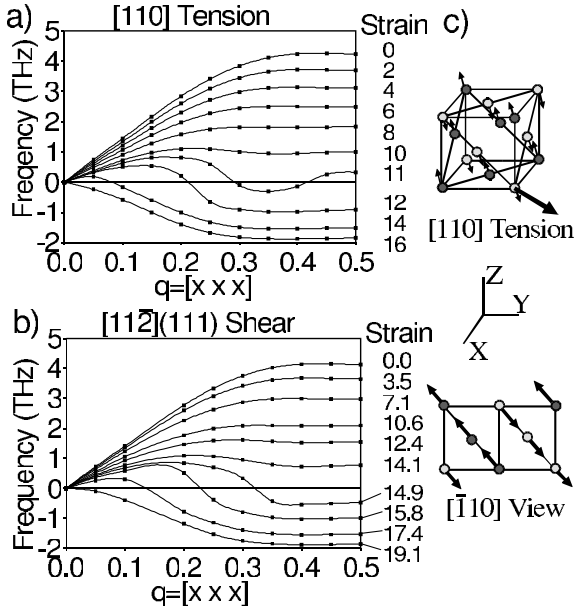

FIG. 3. Phonon frequencies as a function of strain for (a) [110] tension and (b) $[11\bar{2}](111)$ shear. The curves are labeled according to the applied strain as indicated on the right side of the figure. Lines are spline fits which are guides to the eye. In both cases the crystallography of the instability is the same. A schematic illustrating the zone edge instability is shown in (c).

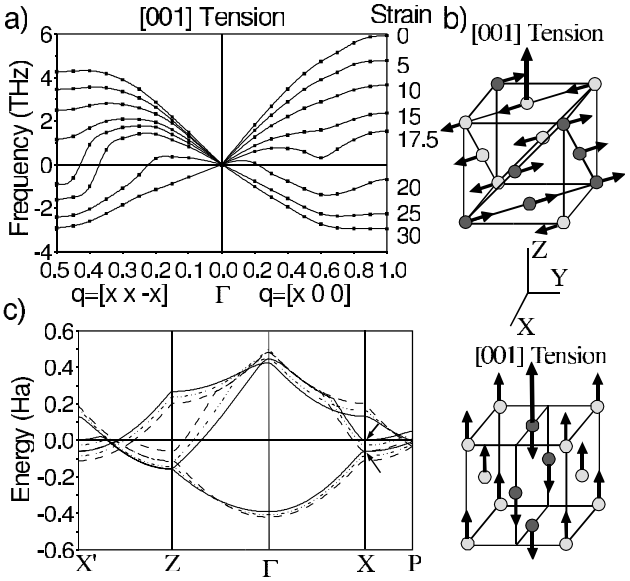

FIG. 4. (a) Phonon frequencies as a function of strain for [001] tension. (b) Schematic of the instabilities. (c) Band structure for 0% (dashed line), 10% (dot-dashed line), 20% (solid line) strains. Coordinates of symmetry points in units of $2\pi/a$, $X = (100)$; $Z = (001)$; $P = (a/2c)$; $X' = (a/c)$. At the instability strain ($\sim 20\%$), the bottom of the second band at the X point reaches the Fermi level as emphasized by the arrows.

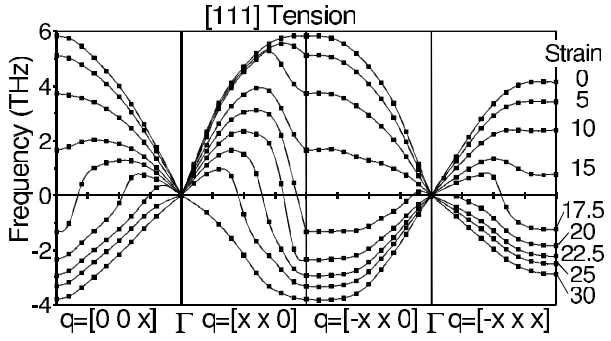

FIG. 5. Phonon frequencies as a function of strain for [111] tension. At 20% strain, the initial slope in the $[\bar{1}10]$ direction becomes imaginary indicating that the crystal is elastically unstable.

seen by examining the Fermi surface. As the crystal is strained in the [001] direction the extent of the intrusion of the Fermi surface into the second zone in the [100] and [010] directions decreases. At the strain which corresponds to the phonon instability this pocket of electrons completely vanishes, destabilizing the structure. A similar though less dramatic event occurs during [110] tension at the strain corresponding to the phonon instability

Finally, the case of [111] tension is the most complex. Phonon instabilities develop along four different high symmetry directions. In all cases, the phonons first become unstable between 15% and 17.5% strain. Analysis of the eigenvectors of the dynamical matrix leads to the result that all the phonon instabilities are shear in character with atomic displacements in the [111] direction but with different shear planes as shown in Table II. We also note that around 20% strain the long wavelength wave velocity becomes imaginary in the $[\bar{1}10]$ direction. This indicates the material is elastically unstable. By computing the elastic constants as a function of strain along the loading path we have been able to locate the same elastic instability using the conditions of internal stability [20]. This instability is orthogonal to the loading direction and is thus not revealed by the relaxed stress-strain curve.

For the four cases studied here we have shown that even in tensile loading the failure mode of Al is shear in nature. Al is known to be ductile even at low temperatures and does not exhibit cleavage fracture. This is consistent with our results which further suggest that shear failure is an inherent property of Al even in an initially dislocation-free perfect crystal.

The authors would like to thank Mr. Weidong Luo for helpful discussions. This work was supported by the Director, Office of Energy Research, Office of Basic Energy Sciences, Materials Sciences Division of The U.S. Department of Energy under Contract No. DE-AC03-76SF00098. Portions of this work were also performed under the auspices of the U.S. Department of Energy by the University of California, Lawrence Livermore National Laboratory, under Contract No. W-7405-Eng-48.

*Electronic address: jwmorris@uclink4.berkeley.edu

[1] A. Kelly and N. H. Macmillan, *Strong Solids* (Clarendon Press, Oxford, 1986), 3rd ed., pp. 1–56.
[2] J.W. Morris, Jr., C. R. Krenn, D. Roundy, and Marvin L. Cohen, in *Phase Transformations and Evolution in Materials*, edited by P. E. Turchi and A. Gonis (TMS, Warrendale, PA, 2000), pp. 187–207.
[3] C. R. Krenn *et al.*, Phys. Rev. B **65**, 134111 (2002).
[4] While an instability can be characterized by its eigenmodes, in general these only describe how the system will behave in nearby regions of the generalized coordinate space. As such, the manner in which the instability is finally resolved can be a complex inhomogeneous process which is best studied by molecular dynamics.
[5] In some respects an elastic instability can be thought of as a phonon instability with a vanishing wave vector; however, we will reserve the term phonon instability for cases in which the unstable wave vectors are away from the zone center.
[6] C. R. Krenn, J.W. Morris, Jr., S.-H. Jhi, and J. Ihm, in *Hard Coatings Based on Borides, Carbides, and Nitrides*, edited by A. Kumar, Y.-W. Chung, and R.W. J. Chia (TMS, Warrendale, PA, 1998), pp. 379–388.
[7] Seung-Hoon Jhi, S. G. Louie, Marvin L. Cohen, and J.W. Morris, Jr., Phys. Rev. Lett. **87**, 075503 (2001).
[8] Ju Li and S. Yip, Comput. Model. Eng. Sci. **3**, 219 (2002).
[9] D. C. Wallace, *Thermodynamics of Crystals* (J. Wiley, New York, 1972), pp. 32–41.
[10] S. Baroni, P. Giannozzi, and A. Testa, Phys. Rev. Lett. **58**, 1861 (1987); X. Gonze and J.-P. Vigneron, Phys. Rev. B **39**, 13 120 (1989).
[11] S. Goedecker, M. Teter, and J. Hutter, Phys. Rev. B **54**, 1703 (1996).
[12] D. M. Ceperley and B. J. Alder, Phys. Rev. Lett. **45**, 566 (1980).
[13] J. P. Perdew and Y. Wang, Phys. Rev. B **45**, 13 244 (1992).
[14] X. Gonze *et al.*, Comput. Mater. Sci. **25**, 478–492 (2002).
[15] N. Marzari, Ph.D. thesis, Cambridge University, 1996.
[16] H. J. Monkhorst and J. D. Pack, Phys. Rev. B **13**, 5188 (1976).
[17] D. Roundy, C. R. Krenn, Marvin L. Cohen, and J.W. Morris, Jr., Philos. Mag. A **81**, 1725 (2001).
[18] D. Roundy, C. R. Krenn, Marvin L. Cohen, and J.W. Morris, Jr., Phys. Rev. Lett. **82**, 2713 (1999).
[19] R. Hill, Math. Proc. Cambridge Philos. Soc. **77**, 225 (1975); R. Hill and F. Milstein, Phys. Rev. B **15**, 3087 (1977).
[20] J.W. Morris, Jr. and C. R. Krenn, Philos. Mag. A **80**, 2827 (2000).
[21] X. Gonze, Phys. Rev. B **55**, 10 337 (1997); X. Gonze and C. Lee, Phys. Rev. B **55**, 10 355 (1997).
[22] *Thermal Expansion: Metallic Elements and Alloys*, edited by Y. S. Touloukian *et al.* (IFI/Plenum, New York, 1975), pp. 2–12.
[23] G. N. Kamm and G. A. Alers, J. Appl. Phys. **35**, 327 (1964).
[24] R. Stedman and G. Nilsson, Phys. Rev. **145**, 492 (1966).
[25] Shigenobu Ogata, Ju Li, and S. Yip, Science **298**, 807 (2002).
[26] Subsequent investigation has revealed that the discrepancies between [18,25] were due to the low precision of the pseudopotential used in [18].
[27] D. M. Clatterbuck and J.W. Morris, Jr. (unpublished).